X-shooter spectroscopy of Liller 1 giant stars★

D. A. Alvarez Garay[1,2], C. Fanelli[2], L. Origlia[2], C. Pallanca[1,2], A. Mucciarelli[1,2], L. Chiappino[1,2], C. Crociati[1,2], B. Lanzoni[1,2], F. R. Ferraro[1,2], R. M. Rich[3], and E. Dalessandro[2]

https://arxiv.org/abs/2404.14130

ABSTRACT

We present the first comprehensive chemical study of a representative sample of 27 luminous red giant branch (RGB) stars belonging to Liller 1, a complex stellar system in the Galactic bulge. This study is based on medium-resolution near-infrared spectra acquired with X-shooter at the Very Large Telescope. We found a subpopulation counting 22 stars with subsolar metallicity ($\langle$[Fe/H]$\rangle$ = -0.31 ± 0.02 and 1σ dispersion of 0.08 dex) and with enhanced [α/Fe], [Al/Fe], and [K/Fe] that likely formed early and quickly from gas that was mainly enriched by type II supernovae, and a metal-rich population counting 5 stars with supersolar metallicity ($\langle$[Fe/H]$\rangle$ = $+0.22 \pm 0.03$ and 1σ dispersion of 0.06 dex) and roughly solar-scaled [α/Fe], [Al/Fe], and [K/Fe] that formed at later epochs from gas that was also enriched by type Ia supernovae. Moreover, both subpopulations show enhanced [Na/Fe], as in the bulge field, about solar-scaled [V/Fe], and depletion of [C/Fe] and $^{12}C/^{13}C$ with respect to the solar values. This indicates that mixing and extra-mixing processes during the RGB evolution also occur at very high metallicities. Notably, no evidence of a Na–O anticorrelation, which is considered the fingerprint of genuine globular clusters, has been found. This challenges any formation scenarios that invoke the accretion of a molecular cloud or an additional stellar system onto a genuine globular cluster. The results of this study underline the strong chemical similarity between Liller 1 and Terzan 5 and support the hypothesis that these complex stellar systems might be fossil fragments of the epoch of Galactic bulge formation.

Introduction

- Liller 1 : a massive stellar system in the Galactic bulge located at 0.8kpc from the Galactic center
    - high absolute and differential reddening
        - $E(B-V) \approx 4.5mag,\ \delta E(B-V) = -0.57 \sim +0.37mag$
- There **are two subpopulations within Liller 1** , which is shown by color-magnitude diagram
    - A main 12Gyr old, subsolar subpopulation
    - A younger (1-3Gyr), supersolar subpopulation
- The first Liller 1 metallicity distribution by MUSE shows (Crociati et al.2023)
    - A dominant metal-poor component with a peak at [Fe/H] ~ -0.5dex ($\sigma \sim 0.2dex$)
    - A metal-rich component with a peak at [Fe/H] ~ 0.3dex ($\sigma \sim 0.2dex$)

→ Liller 1 is another complex stellar system of the bulge, **hosting multi-age and multi-iron stellar subpopulations** similarly to Terzan 5 (another massive globular cluster)

→ **A proper spectroscopic screening of its elemental abundances is urgent**

Observations

- 34 bright giant stars in Liller 1 were spectroscopically observed by X-shooter at VLT.
    - R ≈ 8000, 1.15 – 2.37 μm
- The spectra were reduced with ESO X-shooter pipeline version 3.1.0 to obtain 2D spectra
- The 1D spectrum was extracted manually in order to optimize the location and extension

Stellar membership from proper motions

- Liller 1 population was distinguished from the Galactic field by the proper motion distributions of Gaia DR3.
- Criteria : proper motion vector is located within $3 \times \sigma_{PM}$ ($\sigma_{PM} \approx 0.5\ mas/yr$) (Fig.2)
    - 27/34 stars were satisfied.

Spectral analysis

- Radial velocities are determined via cross-correlation technique
- The chemical abundances were determined via spectral synthesis.
    - Radiative transfer code URBOSPECTRUM (Alvarez & Plez 1998; Plez 2012)
    - MARCS models atmospheres (Gustafsson et al. 2008)
    - Atomic data : VALD3 compilation
    - Molecular data : from the website of B.Plez
- A photometric estimate **of the stellar temperature and gravity** was derived from suitable isochrones by Bressan et al. (2012) by matching the old (12 Gyr) and young (1, 2, 3 Gyr) components of Liller 1 at [Fe/H] ≈ – 0.3 and [Fe/H] ≈+0.3. → Table2.
- For the chemical analysis, they compiled a list of suitable atomic lines over the entire J, H, K spectral range (Na I, Mg I, Al I, Si I, K I, Ca I, Ti I, V I, Fe I)
    - OH molecular lines and CO bandheads were also used for O and C abundances

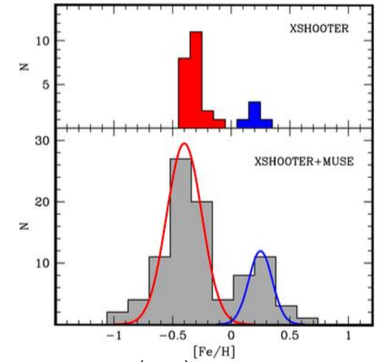

Fig.4 (left)

Results

- Two components were found. → Fig.4
    - 22 stars : metal-poor [Fe/H] = -0.31 ± 0.02
    - 5 stars : metal-rich [Fe/H] = $+0.22 \pm 0.03$
- The metal-poor subpopulation shows some enhanced (by a factor of 2 – 3 on average) **[α/Fe]**, **[Al/Fe]**, and **[K/Fe]** with respect to the solar values (α *elements* : O, Mg, Si, Ca, Ti)
- The **[V/Fe]** abundance ratio is about solar at all metallicities
- [Na/Fe] is enhanced in the metal-poor and metal-rich subpopulations
- The metal-poor/rich components of Liller 1 are both **significantly depleted in [C/Fe]** and in the **$^{12}C/^{13}C$ isotopic ratio** with respect to the solar values. → Fig.6
- No specific trend is evident for [Al/Fe] vs [O/Fe], [Na/Fe] vs [O/Fe] and [Na/Fe] vs [C/Fe] → Fig. 7

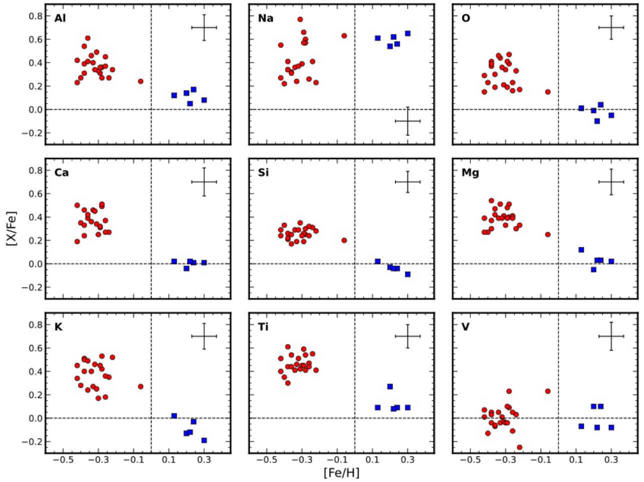

Fig. 5. Behavior of [Al/Fe], [Na/Fe], [O/Fe], [Ca/Fe], [Si/Fe], [Mg/Fe], [K/Fe], [Ti/Fe], and [V/Fe] as a function of [Fe/H] for the metal-poor (filled red circles) and metal-rich (filled blue squares) subcomponents we analyzed. The typical error bars of the measurements are reported in the right corner of each panel. The dashed vertical and horizontal lines denote the corresponding zero values.

Discussion and conclusions

- The metal-poor component with subsolar metallicity and enhanced **[α/Fe]**, **[Al/Fe]**, and **[K/Fe]**

    → consistent with the ordinal scenario
    - the metal-poor subpopulation : early enriched by type II SNe
    - young age, metal-rich subpopulation : enriched by the ejecta by type Ia SNe on longer timescales
- significantly depleted [C/Fe] and 12C/13C isotopic ratio with respect to the solar values

    → consistent with mixing and extra-mixing processes during RGB
- **Na-O anticorrelation** typically seen in globular clusters (GC, Carretta et al. 2009) **is not observed**.

    →challenges the formation scenarios of GC
    - The accretion of a giant molecular cloud by a genuine GC
    - The merger of two GCs
- Liller 1 and Terzan 5 are likely complex stellar systems that have **formed and evolved within the bulge.**

Both are very massive ($\sim 10^6 M_\odot$), but might be more massive in the past, allowing them to retain the SN ejecta and possibly to self-enrich as shown by the recent chemical evolution modeling of Terzan 5 presented in Romano et al. (2023)

- They could be fossil fragments of the pristine clumps of stars and gas that may have contributed to forming the early bulge

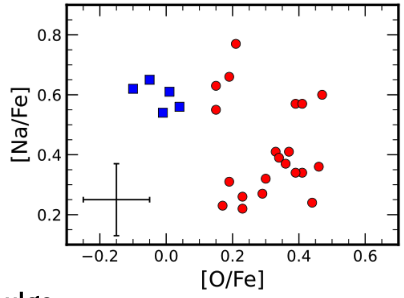

Fig.7 (middle)

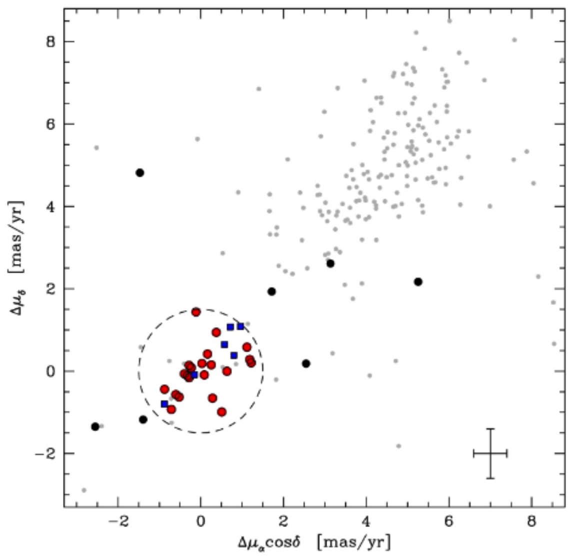

Fig. 2. Vector point diagram of the stars with $G < 19$ in the direction of Liller 1 (small gray circles), showing the RA and Dec components of the *Gaia* DR3 proper motions referred to the systemic values quoted by Vasiliev & Baumgardt (2021). The large dashed circle is centered on (0, 0) and has a radius equal to $3 \times \sigma_{\rm PM}$, with $\sigma_{\rm PM} = 0.5\,{\rm mas\,yr^{-1}}$ being the proper motion dispersion of Liller 1 member stars. The spectroscopic targets are plotted with large symbols: large black dots show those classified as Galactic field interlopers due to their discordant proper motions, and large red dots and blue squares show the likely metal-poor and metal-rich members, respectively. The typical error bar is reported in the bottom right corner.

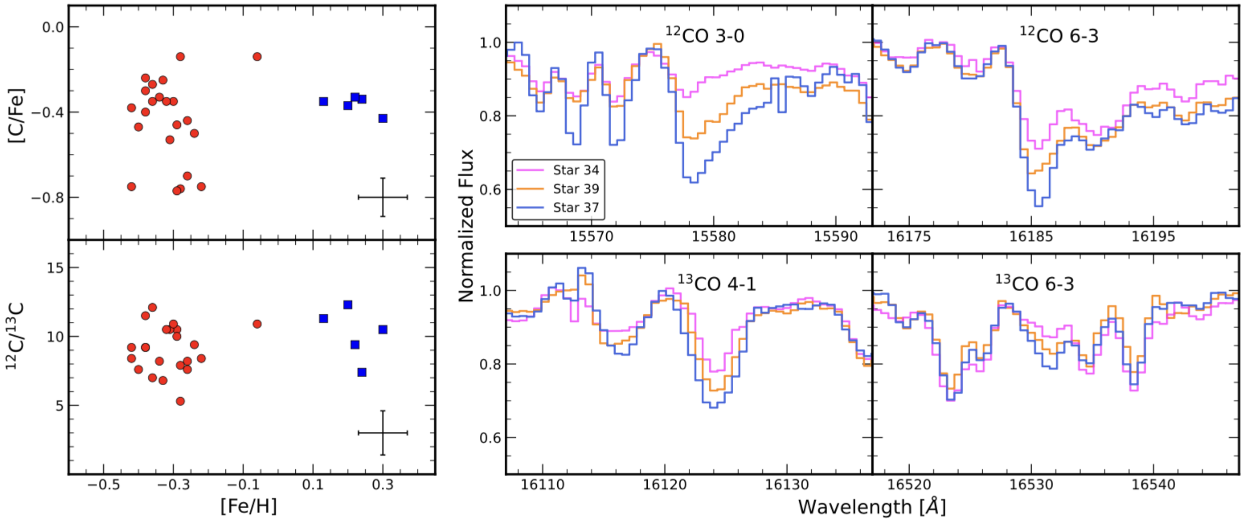

Fig. 6. Carbon measurements for the observed stars. Left panel: behavior of [C/Fe] (top) and ^{12}C/^{13}C ratio (bottom) as a function of [Fe/H] for the metal-poor (filled red circles) and metal-rich (filled blue squares) components of Liller 1. The error bars in the bottom right corners represent the typical error associated with the measurements. Right panel: ^{12}CO 3−0 and 6−3 (top) and ^{13}CO 4−1 and 6−3 (bottom) roto-vibration molecular bandheads in the H band, as observed in three metal-poor stars with similar stellar parameters, iron abundances, and ^{12}C/^{13}C isotopic ratios, but different carbon abundances.

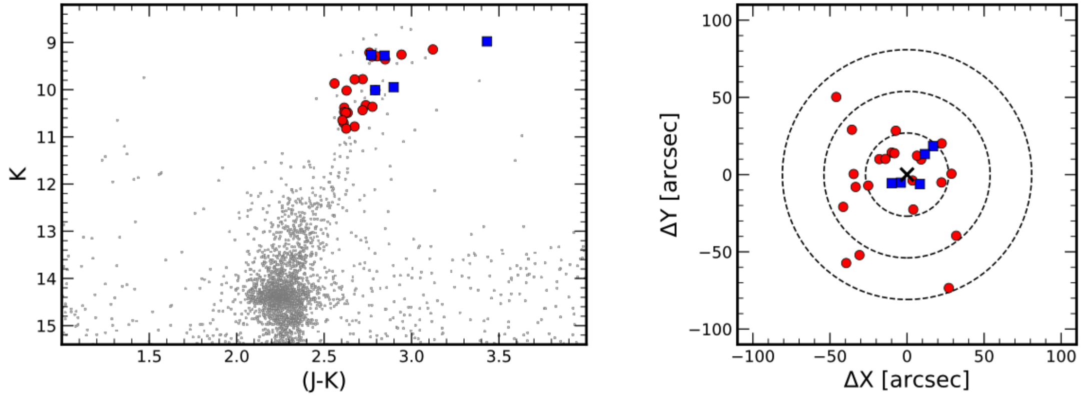

Fig. 3. Photometric properties and spatial location of the observed stars. Left panel: K, $(J-K)$ CMD of Liller 1 (gray dots). The likely metal-poor (filled red circles) and metal-rich (filled blue squares) member stars for which we measured chemical abundances (see Sect. 5.2) from the observed X-shooter spectra are indicated. Right panel: distribution of these stars (same symbols) on the plane of the sky with respect to the cluster center, marked with the black cross and located at RA = 263°.3523333, Dec = −33°.3895556. The radii of the dashed black circles are equal to 5, 10, and 15 times the core radius $r_c = 5''.39$ (Saracino et al. 2015).

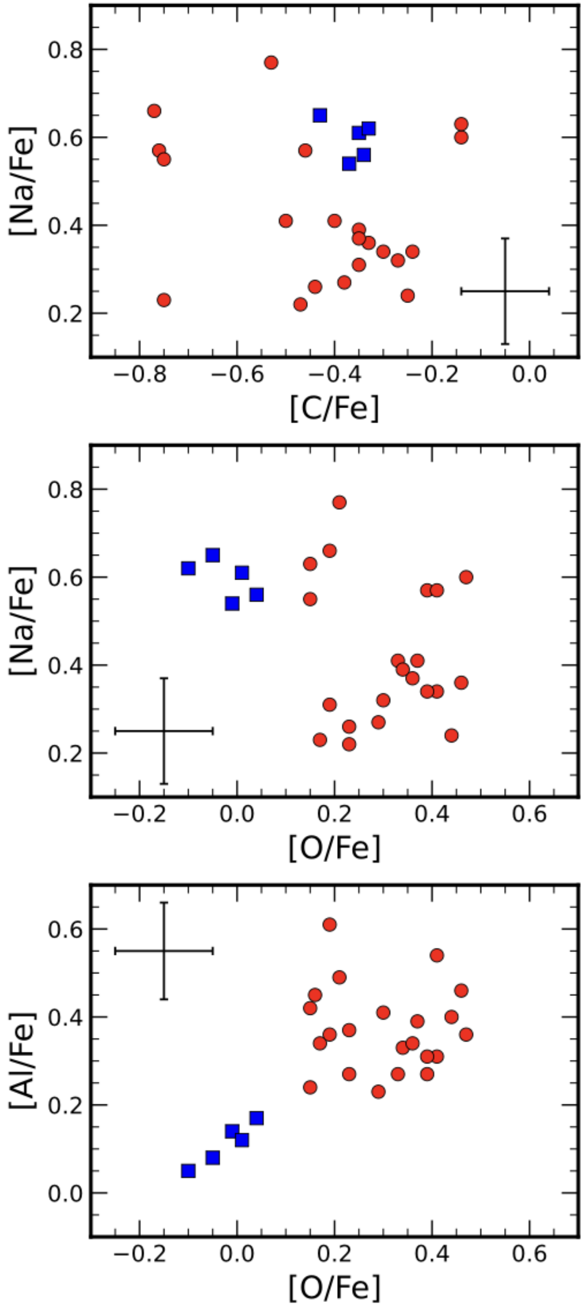

Fig. 7. Behavior of [Na/Fe] vs [C/Fe] (top panel) and vs [O/Fe] (middle panel), and of [Al/Fe] vs [O/Fe] for the metal-poor (filled red circles) and metal-rich (filled blue squares) member stars of Liller 1. The typical measurement errors are reported in one corner of each panel.

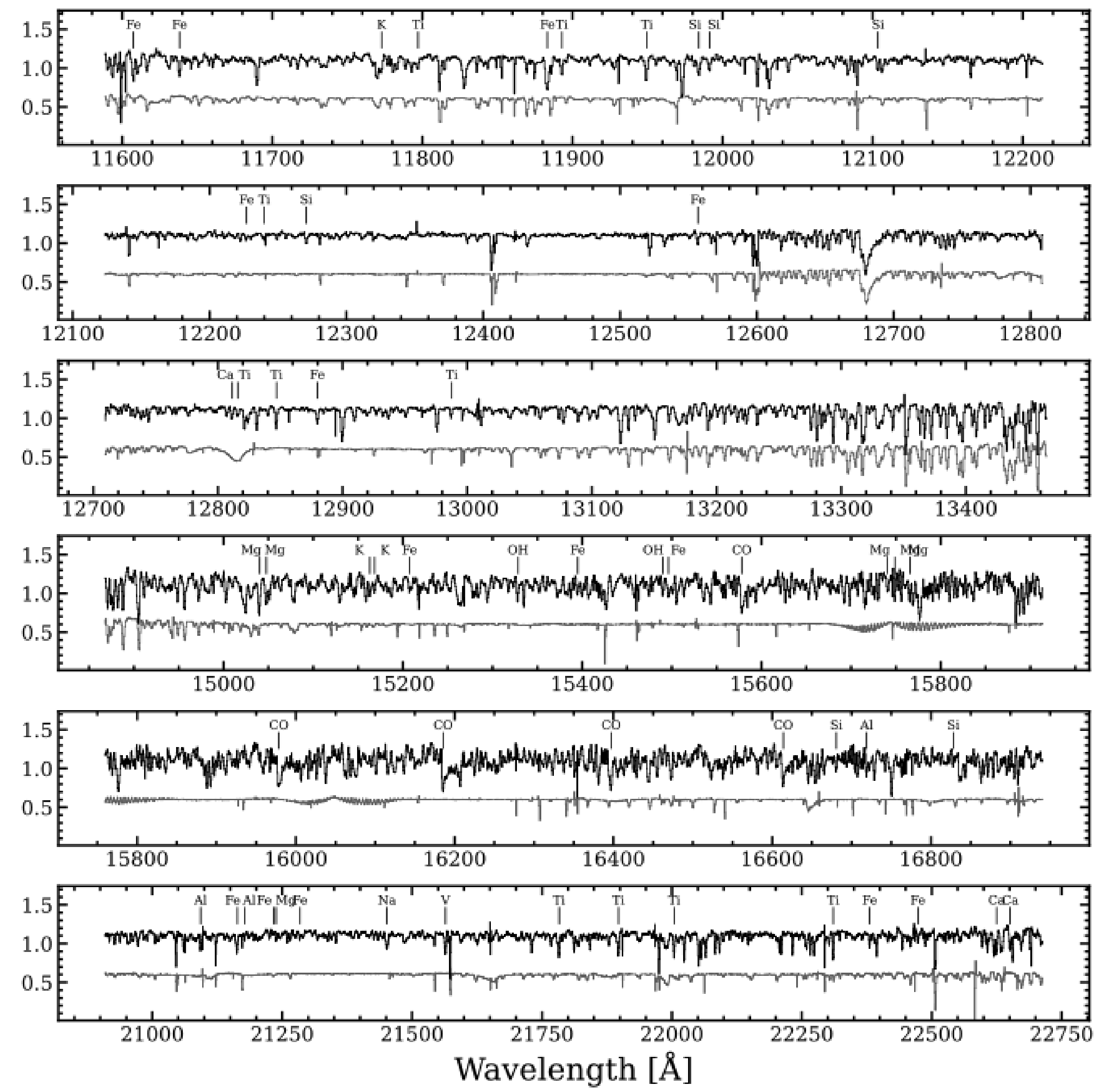

Fig. 1. Portions of the X-shooter spectrum for a giant star with a temperature of 3400 K across the *J*, *H*, and *K* bands (featuring X-shooter orders 22, 21, 20, 17, 16, and 12 from top to bottom). Some lines of interest for the chemical analysis are also marked. In each panel, the upper spectrum in black is the stellar normalized spectrum corrected for radial velocity, and the lower gray spectrum shows the telluric absorption.

Table 1. Observed stars in Liller 1.

ID	RA [Deg]	Dec [Deg]	*J* [mag]	*K* [mag]	Distance [arcsec]
20	263.3413160	−33.3917580	12.27	9.15	34.3
24	263.3580030	−33.3844380	12.03	9.26	25.0
27	263.3463770	−33.3867450	11.97	9.22	20.6
31	263.3386050	−33.3953320	12.10	9.29	46.4
34	263.3370940	−33.3755720	12.07	9.30	68.0
35	263.3561440	−33.3858760	12.12	9.28	17.6
37	263.3408550	−33.3894200	12.21	9.36	34.6
39	263.3619960	−33.3893320	12.20	9.26	28.9
45	263.3540437	−33.3894655	12.02	9.48	5.3
48	263.3509838	−33.3909300	12.41	8.98	6.6
62	263.3659950	−33.4061700	12.50	9.75	72.6
66	263.3614350	−33.4098700	12.50	9.78	78.3
68	263.3392510	−33.4054300	12.46	9.78	69.5
71	263.3535490	−33.3906021	12.43	9.87	5.2
74	263.3490706	−33.3910950	12.80	10.01	11.4
79	263.3491370	−33.3856470	12.65	10.02	17.4
85	263.3551136	−33.3912034	12.84	9.95	10.3
88	263.3537148	−33.3957827	12.80	10.01	22.9
98	263.3560121	−33.3878820	12.98	10.41	12.6
100	263.3440470	−33.3914300	13.00	10.38	26.2
103	263.3554470	−33.3868030	13.07	10.33	13.4
104	263.3478150	−33.3866650	13.13	10.49	17.3
108	263.3515430	−33.4021070	13.06	10.31	45.5
109	263.3548662	−33.3878013	13.08	10.60	9.8
115	263.3599230	−33.3909680	13.14	10.36	22.9
120	263.3599690	−33.3839110	13.16	10.44	30.2
121	263.3404830	−33.3814510	13.09	10.47	46.1
124	263.3421180	−33.4040030	13.11	10.49	60.6
126	263.3496644	−33.3857118	13.32	10.71	16.0
132	263.3630190	−33.4004900	13.25	10.65	50.8
136	263.3545365	−33.3861169	13.46	10.78	13.8
145	263.3499870	−33.3816380	13.45	10.83	29.3
148	263.3529737	−33.3828074	13.48	11.15	24.1
149	263.3629250	−33.4037590	13.50	10.85	60.5

34stars

Table 2. Temperatures, RVs and chemical abundances for the observed stars in Liller 1.

ID	T_{eff}	RV	[Fe/H]	[C/H]	[O/H]	[Na/H]	[Mg/H]	[Al/H]	[Si/H]	[K/H]	[Ca/H]	[Ti/H]	[V/H]	^{12}C/^{13}C
	[K]	[km s^{-1}]	7.50	8.56	8.77	6.29	7.55	6.43	7.59	5.14	6.37	4.94	3.89	89
20	3400	52	−0.28 ± 0.08	−0.42 ± 0.10	+0.19 ± 0.06	+0.32 ± 0.07	+0.12 ± 0.10	+0.08 ± 0.10	+0.02 ± 0.08	+0.14 ± 0.10	+0.21 ± 0.10	+0.26 ± 0.12	−0.05 ± 0.10	5.3 ± 1.4
24	3400	86	+0.24 ± 0.07	−0.10 ± 0.03	+0.28 ± 0.02	+0.80 ± 0.10	+0.27 ± 0.06	+0.41 ± 0.10	+0.20 ± 0.04	+0.21 ± 0.06	+0.25 ± 0.06	+0.33 ± 0.04	+0.34 ± 0.10	7.4 ± 1.7
27	3400	69	−0.38 ± 0.06	−0.78 ± 0.04	−0.01 ± 0.10	+0.03 ± 0.03	+0.16 ± 0.05	+0.01 ± 0.05	−0.17 ± 0.04	+0.02 ± 0.05	+0.08 ± 0.10	+0.23 ± 0.08	−0.33 ± 0.10	9.2 ± 1.2
31	3400	60	−0.24 ± 0.06	−0.74 ± 0.10	+0.09 ± 0.06	+0.17 ± 0.04	+0.06 ± 0.09	+0.03 ± 0.06	+0.07 ± 0.10	+0.11 ± 0.12	+0.03 ± 0.10	+0.31 ± 0.05	−0.21 ± 0.10	9.4 ± 2.0
34	3400	76	−0.28 ± 0.07	−1.04 ± 0.07	+0.11 ± 0.06	+0.29 ± 0.11	+0.23 ± 0.06	−0.01 ± 0.10	−0.03 ± 0.01	+0.25 ± 0.10	+0.23 ± 0.10	+0.13 ± 0.07	−0.19 ± 0.10	7.9 ± 1.3
35	3400	86	+0.20 ± 0.06	−0.17 ± 0.03	+0.19 ± 0.06	+0.74 ± 0.10	+0.15 ± 0.10	+0.34 ± 0.10	+0.17 ± 0.06	+0.07 ± 0.10	+0.16 ± 0.10	+0.47 ± 0.05	+0.30 ± 0.10	12.3 ± 1.8
37	3400	61	−0.33 ± 0.07	−0.58 ± 0.06	+0.11 ± 0.10	−0.09 ± 0.04	+0.18 ± 0.05	+0.07 ± 0.10	−0.14 ± 0.05	−0.06 ± 0.03	+0.13 ± 0.10	+0.13 ± 0.09	−0.37 ± 0.10	6.8 ± 1.6
39	3400	55	−0.29 ± 0.09	−0.75 ± 0.07	+0.12 ± 0.10	+0.28 ± 0.10	+0.19 ± 0.09	+0.02 ± 0.05	−0.03 ± 0.06	–	+0.02 ± 0.10	+0.30 ± 0.07	−0.19 ± 0.10	10.5 ± 1.3
48	3400	42	+0.13 ± 0.08	−0.22 ± 0.06	+0.14 ± 0.10	+0.74 ± 0.10	+0.25 ± 0.10	+0.25 ± 0.06	+0.15 ± 0.05	+0.15 ± 0.10	+0.15 ± 0.10	+0.22 ± 0.07	+0.06 ± 0.10	11.3 ± 1.2
66	3500	99	−0.06 ± 0.05	−0.20 ± 0.05	+0.09 ± 0.06	+0.57 ± 0.10	+0.19 ± 0.04	+0.18 ± 0.10	+0.14 ± 0.06	+0.21 ± 0.10	–	–	+0.17 ± 0.10	10.9 ± 1.5
68	3500	78	−0.36 ± 0.05	−0.63 ± 0.05	−0.06 ± 0.08	−0.04 ± 0.10	+0.06 ± 0.06	+0.05 ± 0.10	−0.19 ± 0.05	−0.12 ± 0.10	+0.03 ± 0.10	+0.18 ± 0.09	−0.43 ± 0.10	7.0 ± 1.6
71	3500	53	−0.40 ± 0.08	−0.87 ± 0.04	−0.17 ± 0.07	−0.18 ± 0.10	−0.13 ± 0.05	−0.13 ± 0.06	−0.07 ± 0.04	−0.12 ± 0.10	−0.05 ± 0.10	−0.05 ± 0.05	−0.53 ± 0.10	7.6 ± 1.0
74	3500	70	+0.30 ± 0.06	−0.13 ± 0.03	+0.25 ± 0.07	+0.95 ± 0.10	+0.32 ± 0.10	+0.38 ± 0.10	+0.21 ± 0.05	+0.11 ± 0.10	+0.31 ± 0.10	+0.39 ± 0.05	+0.22 ± 0.10	10.5 ± 1.8
79	3600	70	−0.22 ± 0.05	−0.97 ± 0.10	−0.05 ± 0.10	+0.01 ± 0.10	+0.11 ± 0.10	+0.12 ± 0.10	+0.06 ± 0.08	+0.30 ± 0.10	–	+0.19 ± 0.08	−0.47 ± 0.10	8.4 ± 1.0
85	3500	61	+0.22 ± 0.07	−0.11 ± 0.10	+0.12 ± 0.06	+0.84 ± 0.10	+0.25 ± 0.05	+0.27 ± 0.10	+0.18 ± 0.04	+0.10 ± 0.10	+0.24 ± 0.10	+0.30 ± 0.10	+0.14 ± 0.10	9.4 ± 1.9
88	3600	72	−0.34 ± 0.08	−0.67 ± 0.04	+0.12 ± 0.10	+0.02 ± 0.10	+0.05 ± 0.10	+0.12 ± 0.08	−0.05 ± 0.04	+0.06 ± 0.10	+0.02 ± 0.07	+0.07 ± 0.04	−0.29 ± 0.10	8.2 ± 1.7
100	3700	68	−0.42 ± 0.08	−1.17 ± 0.07	−0.27 ± 0.08	+0.13 ± 0.10	−0.03 ± 0.10	+0.00 ± 0.08	−0.13 ± 0.05	−0.08 ± 0.06	−0.23 ± 0.10	−0.02 ± 0.08	−0.35 ± 0.10	9.2 ± 1.7
103	3700	40	−0.38 ± 0.07	−0.62 ± 0.04	+0.03 ± 0.06	−0.04 ± 0.10	−0.01 ± 0.10	+0.16 ± 0.05	−0.12 ± 0.05	+0.13 ± 0.10	−0.05 ± 0.10	+0.06 ± 0.04	−0.35 ± 0.10	11.5 ± 2.3
104	3700	57	−0.38 ± 0.06	−0.68 ± 0.05	+0.01 ± 0.07	−0.04 ± 0.10	−0.08 ± 0.10	−0.07 ± 0.05	−0.16 ± 0.10	+0.12 ± 0.10	−0.14 ± 0.10	−0.08 ± 0.10	−0.42 ± 0.10	9.2 ± 1.5
115	3700	57	−0.26 ± 0.09	−0.96 ± 0.10	−0.10 ± 0.10	–	+0.15 ± 0.05	+0.19 ± 0.06	−0.02 ± 0.09	−0.08 ± 0.10	+0.01 ± 0.04	+0.21 ± 0.04	−0.21 ± 0.10	8.2 ± 1.3
120	3700	68	−0.31 ± 0.07	−0.84 ± 0.10	−0.10 ± 0.05	+0.46 ± 0.10	+0.10 ± 0.10	+0.18 ± 0.10	+0.04 ± 0.05	−0.06 ± 0.10	+0.03 ± 0.05	+0.11 ± 0.06	−0.34 ± 0.10	10.5 ± 1.4
121	3700	62	−0.30 ± 0.07	−0.65 ± 0.04	+0.04 ± 0.06	+0.09 ± 0.10	+0.03 ± 0.10	+0.03 ± 0.10	−0.06 ± 0.04	−0.13 ± 0.10	−0.05 ± 0.05	+0.15 ± 0.04	−0.34 ± 0.10	10.9 ± 2.0
124	3700	57	−0.32 ± 0.07	−0.67 ± 0.06	+0.04 ± 0.07	+0.05 ± 0.10	+0.07 ± 0.10	+0.02 ± 0.05	−0.03 ± 0.06	+0.14 ± 0.10	+0.13 ± 0.10	+0.19 ± 0.05	−0.31 ± 0.10	10.5 ± 1.5
126	3700	72	−0.42 ± 0.05	−0.80 ± 0.05	−0.13 ± 0.08	−0.15 ± 0.10	−0.15 ± 0.05	−0.19 ± 0.10	−0.18 ± 0.10	+0.03 ± 0.06	+0.08 ± 0.10	+0.09 ± 0.10	−0.41 ± 0.10	8.4 ± 1.1
132	3700	66	−0.26 ± 0.08	−0.70 ± 0.05	−0.03 ± 0.07	+0.00 ± 0.10	+0.13 ± 0.05	+0.11 ± 0.06	+0.06 ± 0.07	+0.10 ± 0.06	+0.11 ± 0.06	+0.18 ± 0.05	−0.37 ± 0.10	7.6 ± 1.8
136	3800	55	−0.29 ± 0.09	−1.06 ± 0.04	−0.10 ± 0.10	+0.37 ± 0.10	+0.10 ± 0.10	+0.07 ± 0.10	−0.10 ± 0.10	+0.16 ± 0.10	+0.03 ± 0.10	+0.16 ± 0.07	−0.33 ± 0.10	10.0 ± 1.5
145	3800	74	−0.36 ± 0.07	−0.71 ± 0.07	−0.17 ± 0.06	−0.05 ± 0.10	+0.11 ± 0.05	+0.25 ± 0.05	−0.11 ± 0.06	+0.13 ± 0.10	+0.06 ± 0.10	+0.08 ± 0.10	−0.42 ± 0.10	12.1 ± 3.1

Notes. The adopted solar abundances for the measured chemical elements are from Magg et al. (2022) and they are reported in the header of each element abundance column.